ACADEMIA ROMÂNĂ
Revue Roumaine de Chimie
https://www.icf.ro/rrch/

Rev. Roum. Chim.,
2024, *69*(5–6), 247–253
DOI: 10.33224/rrch.2024.69.5-6.02

Dedicated to Professor Vasile Pârvulescu
on the occasion of his 70th anniversary

EXPERIMENTAL AND THEORETICAL ECD STUDY OF THE 7-METHOXYCOUMARIN-3-CARBOXYLIC ACID BINDING TO BSA

Cristina TABLET,[a] Iulia MATEI,[b] Sorana IONESCU [c] and Mihaela HILLEBRAND[c,*]

[a]Faculty of Pharmacy, "Titu Maiorescu" University, Bd. Gh. Sincai 16, Bucharest, Roumania
[b]"Ilie Murgulescu" Institute of Physical Chemistry of the Roumanian Academy,
202 Splaiul Independentei, 060021 Bucharest, Roumania
[c]Department of Physical Chemistry, University of Bucharest, Bd. Regina Elisabeta 4-12, 030018, Bucharest, Roumania

Received February 2, 2024

We report induced circular dichroism (ICD) experimental data on 7-methoxycoumarin-3-carboxylic acid (MCCA) binding to bovine serum albumin (BSA), correlated with electronic circular dichroism (ECD) simulated spectra. The induced chirality and corresponding dichroic signal can be explained by the twisting and steric hindrance of the bound MCCA ligand in the protein pocket. A more general view on the influence that the two intramolecular degrees of freedom of the ligand have on the features of the ECD spectrum is provided, as well as a method to estimate the bound conformation of the ligand. The dependence of the theoretically calculated rotatory strength on the dihedrals between different molecular fragments is discussed. Good correlations with the ICD experimental data are obtained.

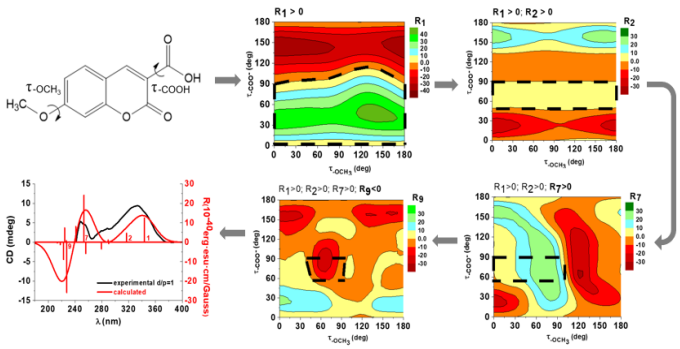

INTRODUCTION

Coupling of the experimental electronic circular dichroism (ECD) spectra of organic molecules with quantum chemically simulated ones has long been used as a method to ascertain the absolute configuration of chiral compounds[1] or, more recently, conformational changes due to steric hindrance in chiral interactions.[2–7] In the presence of proteins, chirality can be induced in optically inactive ligands by conformational adaptation to the binding site, thorough torsional motion, resulting in a bound ligand frozen in a chiral geometry. The molecular asymmetry acquired upon binding leads to the observation of induced circular dichroism (ICD) bands in the range of the electronic absorption of the ligand. Differently from absorption bands, ICD bands can have either positive or negative sign, and are very sensitive to conformation. As such, the ICD spectrum of an achiral small molecule that binds to a biopolymer contains valuable structural information on the bound ligand conformation and on the binding

* Corresponding author: mihaela.hillebrand@gmail.com

site, which can be extracted by way of coupling the experimental data with theoretical, simulated spectra. The procedure has already been successfully used for the case of small ligands characterised by one rotational degree of freedom,[8–14] proving to be a relatively simple and handy way of characterising the protein–ligand complex in solution.

In the following, we focus on the capability of this method to predict the conformation of a ligand having a molecular structure characterized by two degrees of freedom that can be changed in the restrictive medium of the protein binding site, providing an ICD signal. A typical such ligand is 7-methoxycoumarin-3-carboxylic acid (MCCA, Fig. 1) having similar structure with the previously studied 3-carboxy coumarin,[9] but also containing a second substituent, a methoxy group. Two hydrophobic pockets, located in subdomains IIA (Sudlow site I) and IIIA (Sudlow site II) of serum albumins, constitute the main binding sites for such aromatic, heterocyclic ligands.[15] Coumarin derivatives can bind to either one of these sites; for example, warfarin binds with high affinity to Sudlow sites I of both serum albumins, human (HSA) and bovine (BSA),[16] while 3-carboxy coumarin binds to Sudlow I site of HSA and to Sudlow site II of BSA.[17]

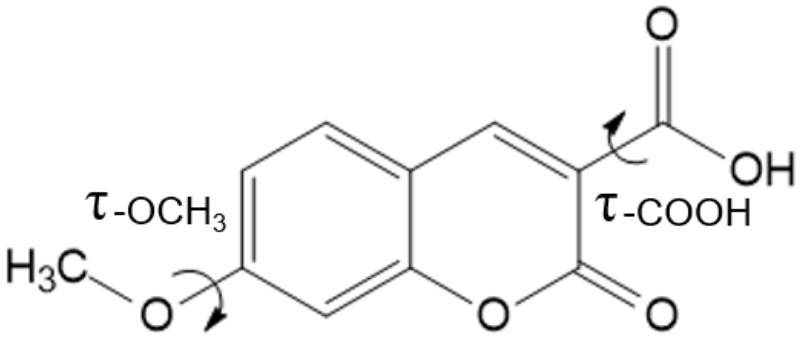

Fig. 1 – Molecular structure of 7-methoxycoumarin-3-carboxylic acid (MCCA).

RESULTS AND DISCUSSION

Induced circular dichroism of BSA-bound MCCA

In solution, in the absence of BSA, no circular dichroism spectrum of achiral MCCA is expected to be observed. This is due to the averaging of spectra from all its possible conformers, resulting in a net zero dichroic signal. When MCCA binds to BSA, a certain non-planar, thus chiral, ligand conformation becomes stabilized in the restrictive medium of the protein pocket, leading to the observation of an ICD signal of bound MCCA (Fig. 2). As it can be seen from Fig. 2, MCCA binding to BSA causes three strong, positive bands to appear in the spectral range between 240 and 380 nm. Their intensity gradually increases with the MCCA concentration, and reaches saturation at drug to protein (d/p) ratios larger than 2. The plot of the CD values at 335 nm *vs.* the MCCA concentration is shown in the inset of Fig. 2. A good fit of these data (r^2 = 0.995, F-stat = 1514) is obtained with equation (1) describing a MCCA–BSA interaction with 1:1 stoichiometry:[18]

$$CD = \frac{k}{2}\left([BSA] + [MCCA] + K^{-1} - \sqrt{([BSA] + [MCCA] + K^{-1})^2 - 4[BSA]\cdot[MCCA]}\right) \quad (1)$$

where k is a constant that equals the ratio of the ICD signal intensity on the concentration of MCCA–BSA complex, and K represents the binding constant. The K value found was $(5.2\pm1.8)\times10^5$ M^{-1}.

At wavelengths below 240 nm, the ICD spectrum of the ligand is subjected to large errors due to small ellipticity values overlapped with the very intense intrinsic dichroic signal of BSA, and due to large protein absorptivities as well.[19] Using a 0.05 cm path length cuvette, at lower protein concentration (2.3×10^{-5} M), and subtracting the protein signal, a negative ICD band at 215 nm can be revealed in the presence of BSA.

We shall show in the following how the experimental ICD data – the position and sign of the three ICD bands, corroborated with molecular modeling results, allows for the estimation of the ligand conformation in the protein binding site.

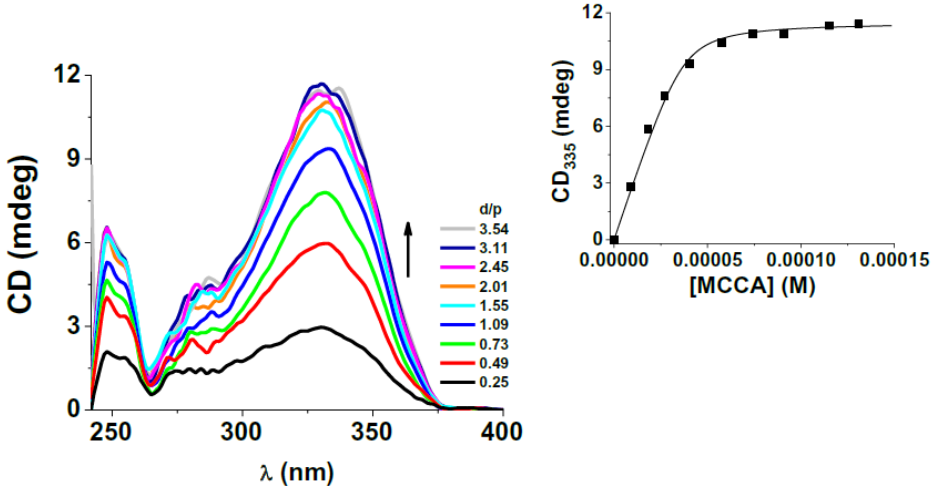

Fig. 2 – The ICD spectra of MCCA in the presence of BSA (3.7×10^{-5} M) at d/p values between 0.25 and 3.54. Inset: The corresponding CD values at 335 nm *vs.* the MCCA concentration. The solid line represents the data fit for a 1:1 stoichiometry of the complex.

Theoretical modeling of the isolated ligand

The first step in the theoretical modeling was to consider the isolated, free ligand. Two torsion angles (τ), *i.e.* the angles formed by the $–COO^–$ and $–OCH_3$ groups with the coumarin ring (Fig. 1), were systematically varied in the range 0–180 deg. Each resulting structure was optimized at the DFT level, allowing all other internal coordinates to relax. The 3D plot of the total energy of deprotonated MCCA (the species present at the pH used in the ICD experiments, see Experimental section) *vs.* the values of the two angles is presented in Fig. 3A. It shows that the most stable MCCA conformation corresponds to $\tau_{–COO-}$ = 60 deg and $\tau_{–OCH3}$ = 0 deg. The energy barriers for the rotation of the $–COO^–$ and $–OCH_3$ groups are 1 kcal/mol (Fig. 3B) and 3.9 kcal/mol (Fig. 3C), respectively, indicating a free rotation in the case of $–COO^–$.

Table 1 summarizes some calculated parameters for the electronic transitions of the most stable conformer, namely the absorption wavelength, oscillator strength and contribution of the monoelectronic transitions to the excited state. As concerns the position and relative intensities of the MCCA absorption bands, the simulated absorption spectrum correlates very well with the experimental one (Fig. 4A). One can notice that the absorption band at longest wavelength is assigned mainly to the *homo→lumo* (*H→L*) transition, whereas the band at 298 nm corresponds to a *H–1→L* transition. For the bands at shorter wavelength there is a contribution from multiple monoelectronic states, so the assignment is less straightforward. Relevant molecular orbitals are depicted in Fig. 4B. It can be noticed that the *H–1*, *L*, *H* and *L+1* orbitals are all localized on the coumarin ring, with contributions from the methoxy group and, except for *L*, from the carboxylate group. This is why conformational changes in these two groups can affect both absorption and circular dichroism spectra.

Table 1

Parameters computed at the B3LYP/6–311+G(d,p) level for deprotonated MCCA in water: absorption wavelength (λ, in nm), oscillator strength (*f*) and configurations contributing to the corresponding excited states (coefficient larger than 0.2) for transitions with $f > 0.1$ down to 200 nm

Transition	λ	f	Assignment
1	347	0.313	0.68(*H→L*)
3	298	0.160	– 0.28(*H–2→L*) + 0.59(*H–1→L*)
8	242	0.108	0.64(*H→L+2*)
17	211	0.108	– 0.26(*H–4→L+1*) + 0.28(*H–1→L+2*) + 0.49(*H→L+5*)
21	201	0.238	0.36(*H–2→L+3*) + 0.27(*H–2→L+4*) + 0.35(*H–1→L+3*) + 0.21(*H–1→L+4*)
22	200	0.249	– 0.27(*H–1→L+1*) + 0.25(*H–1→L+3*) + 0.30(*H→L+6*) + 0.31(*H→L+7*)

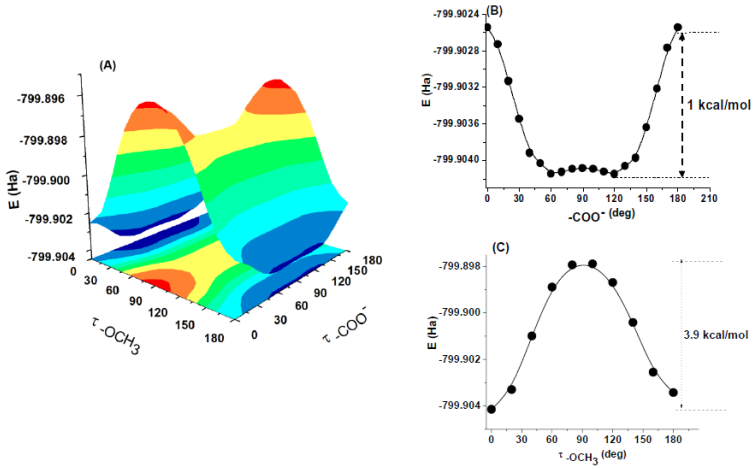

Fig. 3 – The 3D section through the potential energy surface of deprotonated MCCA in water (A) and the 2D sections through the potential energy surfaces of deprotonated MCCA in water when τ_{-OCH3} = 0 deg (B) and τ_{-COO-} = 60 deg (C).

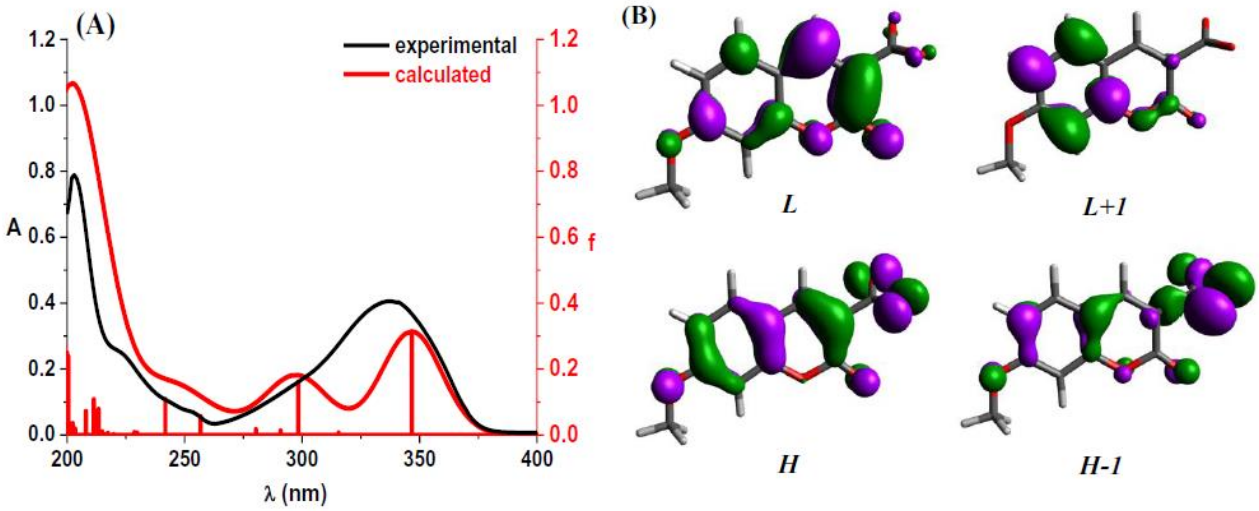

Fig. 4 – (A) Experimental *vs.* calculated (at the B3LYP/6–311+G(d,p) level) absorption spectrum of deprotonated MCCA in water. (B) The *H–1*, *H*, *L* and *L+1* molecular orbitals of the most stable conformer of deprotonated MCCA (τ_{-COO-} = 60 deg, τ_{-OCH3} = 0 deg); isodensity value: 0.04 e/Bohr.^{3}

The most stable conformation of the free ligand in solution is not necessarily the same as the one bound to the protein pocket. Therefore, we have firstly simulated the ECD spectra for different conformations of the free ligand, in the attempt of assigning the bound one based on the best match between theoretical and experimental spectra. We have previously shown that such an approach represents a straightforward method for determining the conformation of ligands whose binding to the protein occurs with the steric hindrance of one degree of freedom.[8–12] However, comparing experimental and theoretical dichroic spectra becomes increasingly difficult as more than one degrees of freedom are altered upon binding. In the case of MCCA, the rotatory strength depends on two torsion angles, τ_{-COO-} and τ_{-OCH3}, and therefore both these geometrical parameters must be considered. One simple way to address this issue is to plot, for each transition relevant in what concerns its wavelength, 2D isosurfaces representing the variation of the rotatory strength *vs.* these torsion angles. Fig. 5A–D present the stepwise procedure we have followed in order to find the MCCA conformation in the BSA pocket.

According to the experimental data, the 335 nm and 290 nm ICD bands are both positive, which corresponds, at the computational level, to positive R_1 and R_2 values, where R_i is the rotatory strength of the transition *i*. The condition $R_1 > 0$ is fulfilled by the values of the torsion angles τ_{-COO-} = 0–90 deg and τ_{-OCH3} = 0–180 deg, enclosed within the dashed area in Fig. 5A. Since R_2 must also be positive, we can further limit these intervals to

τ_{-COO^-} = 45–90 deg and τ_{-OCH3} = 0–180 deg (Fig. 5B). The resulting range of torsion angles can be narrowed further considering the relevant transitions for the experimental ICD bands at 250 nm and 215 nm, *i.e.* transitions 7 and 9, respectively **(**Figs. 5C and D). The relevance of these transitions was established by examining the magnitude of the rotatory strength and global features of the simulated spectra. Applying the same reasoning for $R_7 > 0$ and $R_9 < 0$, we have identified the conformers that can lead to an ECD spectrum that best matches the experimental one. They are characterized by τ_{-COO^-} = 80–90 deg and τ_{-OCH3} = 45–100 deg. An example is given in Fig. 5E, where the negative sign of the experimental band at 215 nm was taken into account (*vide supra*).

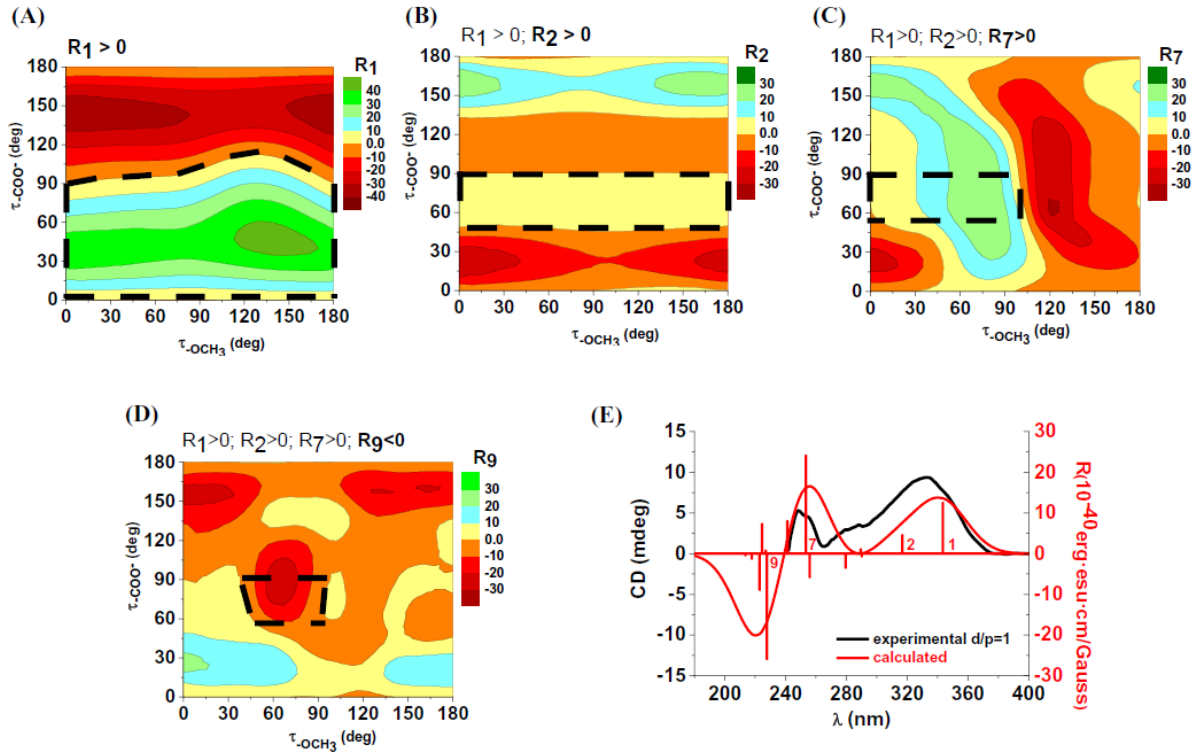

Fig. 5 – The 2D plots of the rotatory strength *vs.* the values of the τ_{-COO^-} and τ_{-OCH3} torsion angles for transitions 1, 2, 7 and 9, which correspond to figures (A), (B), (C) and (D), respectively. The dashed regions correspond to the angle pairs that match the sign conditions written on the top of each figure and imposed by the experimental ICD data for deprotonated MCCA bound to BSA at d/p = 1. (E) The experimental ICD spectrum of the 1:1 MCCA–BSA complex *vs.* the theoretical ECD spectrum of a MCCA conformer characterised by τ_{-COO^-} = 80 deg and τ_{-OCH3} = 60 deg.

Bound ligand. Molecular docking and TDDFT results

For molecular docking, the input geometry of deprotonated MCCA was that of the most stable conformer obtained by DFT. No restriction on the torsion of the $–COO^-$ and $–OCH_3$ groups with respect to the coumarin plane was imposed during the docking procedure. We started by docking the ligand molecule, considering the two main BSA binding sites, Sudlow I, in subdomain IIA, and Sudlow II, in subdomain IIIA.[15] The two torsion angles of interest were measured for the bound conformation of the ligand and the ECD spectrum simulated for those conformations within the intervals previously found by the TDDFT study. The affinities of the most stable complexes in each binding site and the first that matches the spectrum (in bold), together with the corresponding torsion angles can be found in Table 2. As it can be seen, binding to domain IIA of BSA is predicted and the binding mode of MCCA that matches the spectrum corresponds to τ_{-COO^-} = 96 deg and τ_{-OCH3} = 84 deg. To have a better insight on the ligand localization in the protein pocket, the residues within a 3.5 Å diameter sphere around the ligand are indicated as well, while the protein secondary structure is depicted as ribbon (Fig. 6A).

Further, the ligand was isolated from the complex, and a TDDFT calculation was performed at the respective geometry in order to simulate the ECD spectrum. A good match is observed in Fig. 6B

between the experimental spectrum at d/p = 1 and theoretical spectrum of the ligand at the geometry found by molecular docking. The succession of band signs is correctly predicted, and there is a 10 nm shift to longer wavelengths of the simulated spectrum. Thus, one can conclude that the values of the two torsion angles stand as valid criteria for identifying the bound ligand conformation.

Table 2

Scoring function and dihedrals of deprotonated MCCA in the 1:1 BSA complexes; the one with ECD spectra matching the experimental ICD data is given in bold

Protein subdomain	Binding affinity (kcal/mol)	τ_{-COO}-; τ_{-OCH3} (deg)
IIA	–8.53	3; 117
	–6.87	**96; 84**
IIIA	–5.94	105; 95

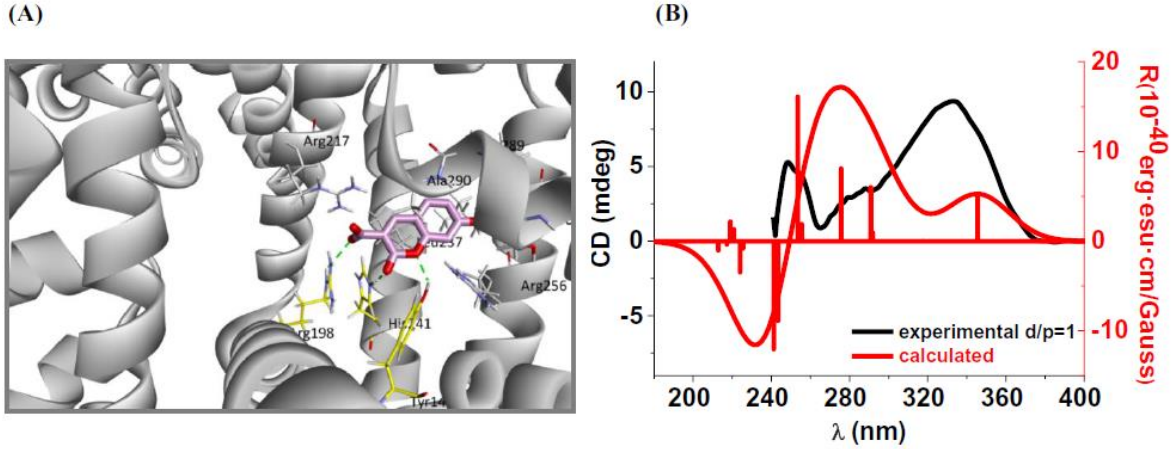

Fig. 6 – (A) Proposed structure of the 1:1 MCCA–BSA complex obtained by molecular docking and supported by a good similarity between the experimental ICD and calculated ECD spectra (B).

EXPERIMENTAL

Circular dichroism and UV-Vis absorption spectroscopies

7-Methoxycoumarin-3-carboxylic acid (MCCA, Sigma, suitable for fluorescence, ≥ 97.0%) and BSA (Sigma-Aldrich, ≥98%, fatty acid free) were used as received, without any further purification. MCCA–BSA solutions at d/p molar ratios in the range 0–3.54 were prepared in pH 7.4 phosphate buffer 0.1 M ensuring a constant protein concentration of 3.7×10^{-5}M.

Circular dichroism and UV-Vis spectra were recorded on a Jasco J-815 CD spectropolarimeter at room temperature using 1 cm path length cuvettes. The spectral range, time constant, scan speed and bandwidth were set at 250–400 nm, 4 s, 100 nm/min and 1 nm, respectively. Each spectrum was signal-averaged three times. A smaller concentration of protein (2.3×10^{-5} M) and a 0.05 cm path length cuvette were used for measurements in the 200–230 nm domain to overcome large protein absorptivities in this range.

Theoretical calculations

Since, according to literature data, coumarin-3-carboxylic acid and its 7-substituted derivatives have a pKa value between 3 and 4,[17,20,21] MCCA was considered deprotonated at pH 7.4. Full geometry optimization of deprotonated MCCA was carried out by density functional theory (DFT) calculations in the frame of the Gaussian09 package,[22] using the B3LYP functional[23–25] and 6-311+G(d,p) basis set. The solvent (water) effect was introduced by the Polarizable Continuum Model.[26] Simulated electronic circular dichroism (ECD) and absorption spectra were obtained by time-dependent DFT (TDDFT) at the B3LYP/6-311+G(d,p) level, and plotted using Gabedit 2.4.6[27] with a full width at half maximum of 15 nm.

Several MCCA conformers were considered by modifying the two dihedral angles, τ_{-COO}- and τ_{-OCH3}, which describe the torsion of the carboxylate and methoxy groups with respect to the coumarin plane (Fig. 1). These angles were kept frozen at selected values in the range 0–180 deg with a step of 10 or 20 degrees and all other internal coordinates were fully optimized. The ECD spectrum was computed for all these conformers and the rotatory strengths corresponding to transitions down to 200 nm were plotted against values of both dihedrals.

The MCCA–BSA complexes were modelled using Autodock 4.2.[28] AutoDockTools[29] and Discovery Studio Visualizer[30] were used for preparing the protein structure and visualizing the complexes. The crystal structure of BSA was taken from the Brookhaven Protein Data Bank,[31] entry code 4JK4. Docking using a grid encompassing the entire protein was firstly performed in order to locate the most probable binding sites of MCCA. Two possible binding sites have been

identified, namely Sudlow sites I and II of albumins, located in subdomains IIA and IIIA, respectively. Smaller grids with dimensions 64×64×64 (in Å) and a spacing of 0.375 Å were then centred on each of the two BSA subdomains, and ten conformers were obtained in each case using the Lamarkian genetic algorithm. Details on the docking procedure can be found elsewhere.[32] The bound MCCA conformers whose ECD spectrum matched the experimental ICD spectrum were selected for discussion.

CONCLUSIONS

The ICD spectra of achiral molecules in hindered environments are difficult to interpret, especially when several intramolecular degrees of freedom exist. Correlating the experimental and quantum chemically computed spectra proves an efficient method in this respect, as it permits extracting information on the stoichiometry and structure of a protein–ligand complex. We conclude that TDDFT-computed ECD spectra of isolated molecules for which all degrees of freedom are varied may be used in conjunction to ICD experimental data in the quest for a molecular level image of small molecule to biopolymer binding. The results are ascertained by docking the ligand molecule to the protein binding site and calculating the ligand ECD spectrum in its bound conformation.

REFERENCES

1. N. Berova, L. Di Bari and G. Pescitelli, *Chem. Soc. Rev.*, **2007**, *36*, 914–931.
2. K. Osawa, H. Tagaya and S. Kondo, *J. Org. Chem.*, **2019**, *84*, 6623−6630.
3. K. Conley, M. A. Whitehead and T. G. M. van de Ven, *Cellulose*, **2017**, *24*, 479−486.
4. E. V. Kundelev, A. O. Orlova, V. G. Maslov, A. V. Baranov and A. V. Fedorov, *Chirality*, **2018**, *30*, 261−267.
5. G. Ionita, S. Mocanu and I. Matei, *Phys. Chem. Chem. Phys.*, **2020**, *22*, 12154–12165.
6. M. Nuskol, P. Šutalo, I. Kodrin and M. Čakić Semenčić, *Eur. J. Inorg. Chem.*, **2022**, *2022*, e202100880.
7. S. Ghidinelli, M. Fusè, G. Mazzeo, S. Abbate and G. Longhi, *Symmetry*, **2022**, *14*, 1108.
8. S. Ionescu, I. Matei, C. Tablet and M. Hillebrand, *Phys. Chem. Chem. Phys.*, **2013**, *15*, 11604–11614.
9. A. Varlan and M. Hillebrand, *J. Mol. Struct.*, **2013**, *1036*, 341–349.
10. I. Matei, S. Ionescu and M. Hillebrand, *Spectrochim. Acta A Mol. Biomol. Spectrosc.*, **2012**, *96*, 709–715.
11. I. Matei, S. Ionescu and M. Hillebrand, *J. Mol. Model.*, **2012**, *18*, 4381–4387.
12. I. Matei, S. Ionescu and M. Hillebrand, *Rev. Roum. Chim.*, **2013**, *58*, 409–413.
13. D. Tedesco and C. Bertucci, *J. Pharm. Biomed. Anal.*, **2015**, *113*, 34–42.
14. L. Zhao, S. Xiao, S. Jiang, Y. Jin, W. Fang and Z. Wang, *J. Mol. Struct.*, **2022**, *1248*, 131530.
15. G. Sudlow, D. J. Birkett and D. N. Wade, *Mol. Pharmacol.*, **1975**, *11*, 824–832.
16. C. Ràfols, S. Amézqueta, E. Fuguet and E. Bosch, *J. Pharm. Biomed. Anal.* **2018**, *150*, 452–459.
17. A. Varlan and M. Hillebrand, *Cent. Eur. J. Chem.*, **2011**, *9*, 624–634.
18. F. Zsila, Z. Bikádi and M. Simonyi, *Biochem. Pharmacol.*, **2003**, *65*, 447–456.
19. S. M. Kelly, T. J. Jess and N. C. Price, *Biochim. Biophys. Acta*, **2005**, *1751*, 119–139.
20. C. Tablet, L. Minea, L. Dumitrache and M. Hillebrand, *Spectrochim. Acta A Mol. Biomol. Spectrosc.*, **2012**, *92*, 56–63.
21. A. Chatterjee and D. Seth, *Photochem. Photobiol.*, **2013**, *89*, 280–293.
22. M. J. Frisch, G. W. Trucks, H. B. Schlegel, G. E. Scuseria, M. A. Robb, J. R. Cheeseman, G. Scalmani, V, Barone, B. Mennucci, G. A. Petersson, H. Nakatsuji, M. Caricato, X. Li, H. P. Hratchian, A. F. Izmaylov, J. Bloino, G. Zheng, J. L. Sonnenberg, M. Hada, M. Ehara, K. Toyota, R. Fukuda, J. Hasegawa, M. Ishida, T. Nakajima, Y. Honda, O. Kitao, H. Nakai, T. Vreven, J. A. Montgomery Jr, J. E. Peralta, F. Ogliaro, M. Bearpark, J. J. Heyd, E. Brothers, K. N. Kudin, V. N. Staroverov, R. Kobayashi, J. Normand, K. Raghavachari, A. Rendell, J. C. Burant, S. S. Iyengar, J. Tomasi, M. Cossi, N. Rega, J. M. Millam, M. Klene, J. E. Knox, J. B. Cross, V. Bakken, C. Adamo, J. Jaramillo, R. Gomperts, R. E. Stratmann, O. Yazyev, A. J, Austin, R. Cammi, C. Pomelli, J. W. Ochterski, R. L. Martin, K. Morokuma, V. G. Zakrzewski, G. A. Voth, P. Salvador, J. J. Dannenberg, S. Dapprich, A. D. Daniels, O. Farkas, J. B. Foresman, J. V. Ortiz, J. Cioslowski and D. J. Fox, Gaussian 09, Revision C.01, 2009, Gaussian, Inc., Wallingford CT.
23. A. D. Becke, *J. Chem. Phys.*, **1993**, *98*, 5648–5642.
24. P. J. Stephens, F. J. Devlin, C. F. Chablowski and M. J. Frisch, *J. Phys. Chem.*, **1994**, *98*, 11623–11627.
25. R. H. Hertwig and W. Koch, *Chem. Phys. Lett.*, **1997**, *268*, 345–351.
26. J. Tomasi, B. Mennucci and R. Cammi, *Chem. Rev.*, **2005**, *105*, 2999–3093.
27. A. R. Allouche, *J. Comput. Chem.*, **2011**, *32*, 174–182.
28. G. M. Morris, R. Huey, W. Lindstrom, M. F. Sanner, R. K. Belew, D. S. Goodsell and A. J. Olson, *J. Comput. Chem.*, **2009**, *30*, 2785–2791.
29. M. F. Sanner, *J. Mol. Graphics Model.*, **1999**, *17*, 57–61.
30. Dassault Systèmes BIOVIA, Discovery Studio Visualizer, Release 4.5, San Diego: Dassault Systèmes, 2016.
31. RCSB Protein Data Bank. http://www.rcsb.org/pdb
32. D. S. Goodsell, G. M. Morris and A. J. Olson, *J. Mol. Recognit.*, **1999**, *9*, 1–5.